1 MASS RESOLUTION

In this section, we investigate how mass resolution affects on halo bias and mass functions. We prepare two samples with 256^3 and 512^3 particles in the cubic box, whose side length is $256h^{-1}$Mpc. Note that both samples are simulated from the same initial density field with the same number of time steps.

We first show comparison of cumulative mass functions in Figure 1. We calculate mean and its error through the bootstrap method, generating 100 samples by choosing halos randomly from an output of the simulation. In the right panel of Figure 1, the mean and its error for the samples of 512^3 particles are indicated as shaded regions and the mean for 256^3 particles indicated as circles. The discrepancy in the mass functions between 256^3 particles and 512^3 particles becomes larger on large halo masses. This is mainly because there are a few large halos and therefore it is more sensitive to the differences in the number of halos. It is possible that samples with higher mass resolutions resolve more small halos and a multiple halos in the samples with 512^3 particles correspond to one larger halo in the 256^3-particles samples. We also see that agreement between the samples of those two mass resolutions is better at lower redshift, possibly because particles are more well clustered at lower redshift. Those differences on mass functions can cause systematic errors on halo bias due to selection of halos.

In Figure 2, we compare halo-matter cross power spectra at various redshifts. Here, we use the same matter density field generated with 256^3 particles for both cases, and we select halos based on the "soft mass-cut" method using the function described below.

$$< N_{halo}(M) >= \frac{1}{2}\mathrm{erfc}(\frac{\log(\mathrm{M_{cut}}/M)}{\sqrt{2}\sigma}), \qquad (1)$$

where we set $\mathrm{M_{cut}} = 10^{13.0}[\mathrm{M_\odot}]$ and $\sigma = 0.5$. Using the soft mass-cut method, we generate 10 samples to compute the cross power spectra and their errors. From now on, we use the same method for halo selections to compute power spectra. Note that the ratio of those cross power spectra is equivalent to the ratio of halo bias. Figure 2 shows the halo bias for 256^3 particles is smaller than for 512^3 particles and they agree well within 2%. This also implies the effect on halo bias due to different mass resolusion is less sensitive compared to the effect on mass functions.

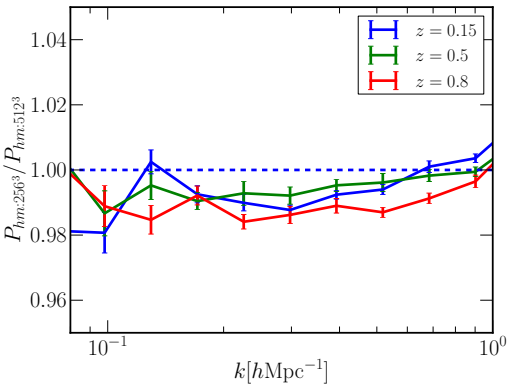

Figure 2. Ratio of halo-matter cross power spectra between the samples of 512^3 and 256^3 particles for various redshifts. The overall agreements are all within 2%. Note that halos are selected based on the "soft masscut" method described in the section.

2 SELECTION OF THE MINIMAL TIME STEPS

The goal in this section is to determine the sufficient time-stepping scheme to resolve halo positions and masses reliably for the future galaxy surveys. We are particularly interested in reducing the number of sub-cycles, because most of computational time is spent in the short-range time solver. In order to quantitatively evaluate different time-stepping schemes, we run a set of convergence tests using smaller simulation boxes. As already explained, our aim is to carry out simulations in approximate $(4h^{-1}\mathrm{Gpc})^3$ volumes with 4096^3 particles, leading to a particle mass of $\tilde{}10^{11}\mathrm{M_\odot}$. We scale down these volumes to $(256h^{-1}\mathrm{Mpc})^3$ with 256^3 particles, which keeps the particle mass unchanged. In addition, we have carried out one simulation with 512^3 particles with exactly the same phases for detailed mass resolution studies. The number of time steps were chosen as 450/5, 300/3, 300/2, 150/3, 150/2, where the first number indicates the number of long time steps and the second number the number of short time steps for each long time step. Note that all the samples used in this section are at redshift $z = 0.15$. After determining our target time-stepping scheme, we do a more detailed examination at various redshifts in the next section. To provide some idea of the variation across all of the choices, we compare observable quantities including mass functions and power spectra in real and redshift spaces, as well as masses and positions of halos matched one by one. Based on

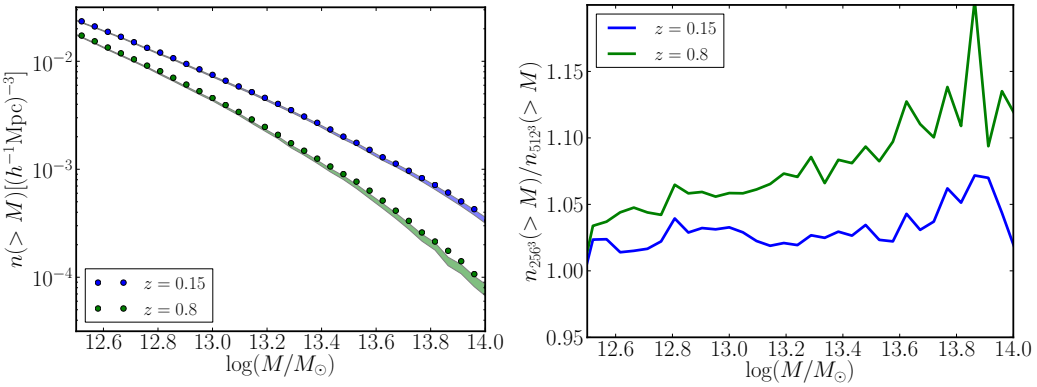

Figure 1. Left: Cumulative mass functions for the simulations of 512^3 and 256^3 particles. Shaded regions are the mean with errors for the samples of 512^3 particles calculated through the bootstrap method. Circles are the mean for 256^3 particles. Right: Ratio of cumulative mass functions between the samples of 512^3 and 256^3 particles. The deviation from one on large halo masses is mainly caused by the fewer number of large halos.

a number of convergence tests, the 300/2 combination turned out to be the best choice.

2.1 Observables

We investigate how mass resolution and the number of time steps affects the observable quantities including mass functions and power spectra.

2.1.1 Time Steps

We first compute mass functions from outputs of different time-stepping schemes, as shown in Figure 3, where we compare simulations with reduced number of time steps to the 450/5 simulation. In Figure 3, we show the ratio $n(>M)/n_{450/5}(>M)$, where $n_{450/5}(>M)$ is a cumulative mass function for the 450/5 simulation and $n(>M)$ is a cumulative mass function for different time steps shown in different colors. Here, we use a fixed linking length of $b = 0.16$ times the mean interparticle separation for all the simulations to identify halos through the friends-of-friends (hereafter, fof) algorithm, and halo masses are assigned based on the number of particles contained in halos. We see that the cumulative mass functions for 150 global steps have smaller amplitudes overall than those for 450 and 300 global steps. This is because a smaller number of time steps makes halos more diffused and the fixed linking length cannot connect some particles in the outputs of 150 global steps whose corresponding particles are connected in the simulations of larger global steps. In addition to the difference

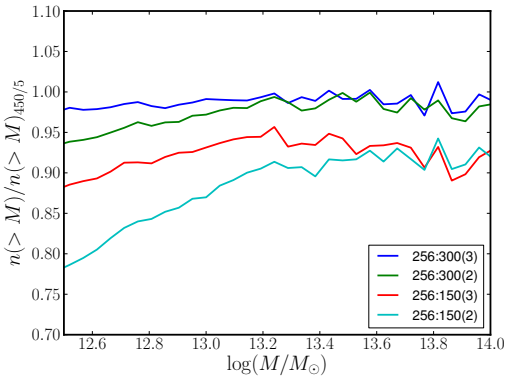

Figure 3. Comparison of cumulative mass functions in different simulations taking the 450/5 as a reference. Lines, from top to bottom, correspond to different time steps, 300/3 (blue), 300/2 (green), 150/3 (red), and 150/2 (cyan) respectively. As shown, the agreement between 300 global steps and the 450/5 is close to one on large halo mass and sub-cycles make differences only on small halo mass.

in global steps, sub-cycles also make the internal structure of halos more diffused and this leads to the suppression on the number of low-mass halos. In Manera et al. 2012 which uses the second-order Lagrangian perturbation theory to generate dark matter fields, they used a longer linking length and reassigned halo masses in order to solve the same problem of having diffused halos. We find that overall agreement between the simulations of 450/5 and 300 global steps on mass functions is sufficient.

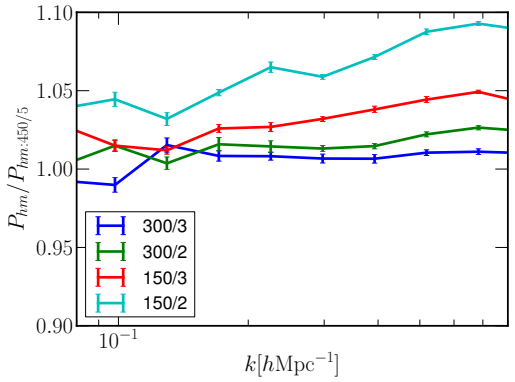

Figure 4. Ratio of halo-matter cross power spectra as a function of time steps with respect to the 450/5. The agreements with the 450/5 are all within 5% on large scales. For 300 global steps, both agree well even on small scales with little difference by sub-cycles. Note that the halos are selected based on the soft mass-cut method with $M_{cut} = 13.0$ and $\sigma = 0.5$.

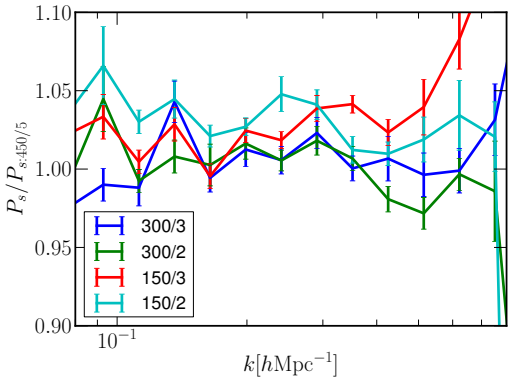

Figure 5. Ratio of redshift-space auto power spectra in different time steps, taking 450/5 as a reference. For 300 global steps, the agreement with the 450/5 is well within 5% on large scales. Here, we select halos based on the soft mass-cut method with $M_{cut} = 13.0$ and $\sigma = 0.5$.

The next measure of interest is the cross power spectra between halos and matter densities, as shown in Figure 4. Figure 4 shows the ratio $P_{hm}/P_{hm,450/5}$ at $z = 0.15$, where $P_{hm,450/5}$ is the cross power spectrum for 450/5 and P_{hm} is the cross power spectrum for other time steps labeled in the figure. To calculate the cross power spectra, we use the output of the 450/5 simulation for the matter densities for all the halo sample. In this way, the ratio $P_{hm}/P_{hm,450/5}$ is equivalent to the ratio of halo bias between the 450/5 and other time-steps, showing systematic errors due to the de-tuned simulations. Here, we use only one realization for the calculations and this is partly why our cross power spectra are noisy on large scales. Another contribution to the noise is the relatively small volume of the simulation box. We see that the agreement between 450/5 and 300 global steps is remarkably good and that the differences are well within 5% on any scales. In addition, we see the systematic error on halo biases for 150 global steps is also within 5% on large scales. This implies that halo bias on large scales is not largely affected by reduction of the time steps.

The final quantitative comparison here is auto power spectra in redshift space. We are particularly interested in how de-tuning affects the velocity fields and therefore, the redshift space. The result is shown in Figure 5 as the ratio $P_s/P_{s,450/5}$, where $P_{s,450/5}$ is the auto power spectrum calculated from the simulation of 450/5 and P_s is the auto power spectrum with reduced number of time steps. Before taking the ratio, we subtracted a Poisson shot noise contribution of $1/n$. We see that the simulations with 150 global steps do not have the same velocity fields as the 450/5 simulation, because their ratios for the redshift-space power spectra between 450/5 and 150 global steps show larger deviations compared to the ratios for halo biases, shown in Figure 4. This implies that the simulations with only 150 global steps have systematic errors in the measurement of the growth factor through redshift-space distortions. For 300 global steps, the agreement with the 450/5 simulation is sufficiently good on large scales.

2.2 Matching

We compare halo properties for those of corresponding halos in different samples. We first show our algorithm for identifying the corresponding halos in two different samples and then compare halo mass, position, and velocity for those matched halos. From the quantitative comparison, we find that the samples with 300 global steps have much less scatter for the baseline of the 450/5 sample than the samples with 150 global steps. In addition to that, we see that the differences between sub-cycles are almost negligible.

2.2.1 Algorithm

Since our simulations all start with the same initial conditions, we match halos in different simulations by matching their particle content. Given a halo in simulation A, we consider the halos in simulation B with the corresponding particles. Given this list of possible matches, we match to the halo with the largest number of common particles. To avoid spurious matches, we also require that the fraction of common particles (relative to simulation A) exceeds a threshold. Figure 6 shows the cumulative fraction of unmatched halos matching the 450/5 to the 300/2 simulation at $z = 0.15$ with various thresholds. As expected, the unmatched fraction increases with increasing threshold and decreasing halo mass. We adopt a threshold of 50% as our default choice.

Since the above matching algorithm is unidirectional, multiple halos in A might be matched to a single halo in B; this happens 1 to 2% of the time with a matching threshold of 50%. We refer to these as multiply-booked halos in what follows. Figure 7 compares halo mass for the matched halos between the 450/5 and the 300/2 simulations at $z = 0.15$. We classified those matched halos into multiply-booked halos and the rest. As shown in Figure 7, the summed halo mass for those multiply-booked halos in the 450/5 is correlated with the corresponding halos in the 300/2 better than the individual halo mass in the 450/5. This implies that those multiply-booked halos in the 450/5 are merged into one halo in the 300/2. Since larger global steps and sub-cycles can capture dynamics better, it is likely that the halos in the 450/5 forms sub-structure earlier than the 300/2 simulation.

Figure 8 shows the number densities of the unmatched halos in the 450/5 matching to the 300/2 at $z = 0.15$. There are three reasons that halos are considered as unmatched. First, if there are no common particles in the halos, we consider them as unmatched. Second, if the fraction of common particles over the total number of particles in each halo is less than 50%, we eliminate these as spurious halos. At last for the case of multiply-booked halos, we remove all but the one with the largest number of common particles. We showed each unmatched number density as a function of halo mass. We only find unmatched halos on low-mass regions for the reason that the halos don't have any common particles. This is because there are some low-mass halos which are identified in one sample but not in another sample due to the way the FoF algorithm define halos. As shown, most of unmatched halos are due to the threshold criterion. We also checked how the number of matched halos is changed as a function of redshift, and we observed that redshift does not affect to the matching algorithm.

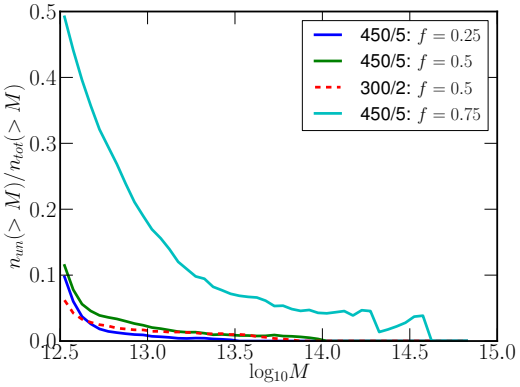

Figure 6. The cumulative fraction of unmatched halos matching the 450/5 to the 300/2 simulation at z=0.15 as a function of halo mass. The solid lines, from top to bottom, correspond to matching thresholds of 75%, 50%, and 25% for the unmatched halos in the 450/5 sample. The dashed line shows the same quantity for the 300/2 sample for a threshold of 50%. As expected, the unmatched fraction increases with decreasing halo mass and increasing threshold. We adopt a threshold of 50% as our default choice.

2.2.2 Halo Properties

Here, we compare halo properties (i.e., halo mass, position, and velocity) for halos matched to those in the 450/5. The comparison of halo mass between the 450/5 and the 300/2 is shown in Figure 7. Figure 7 shows that the halos in the 300/2 simulation tend to be slightly more massive than the corresponding halos in the 450/5. We also compare the halos in the simulation of other time steps to the corresponding halos in the 450/5 and show medians, $\Delta_{65\%}$, and $\Delta_{95\%}$ for the mass differences at different redshifts and for different mass slices in Table 1 and Table 2. The panels in Figure 9, from left to right, show the comparison of halo position and velocity for the matched halos at $z = 0.15$. As shown, the 150 global steps have more scatter in the halo properties and the means differ for the halo mass ratio and the velocity difference. This indicates that the halo structure in these cases is more diffused than the case of the 300 or the 450 global steps. For the 300

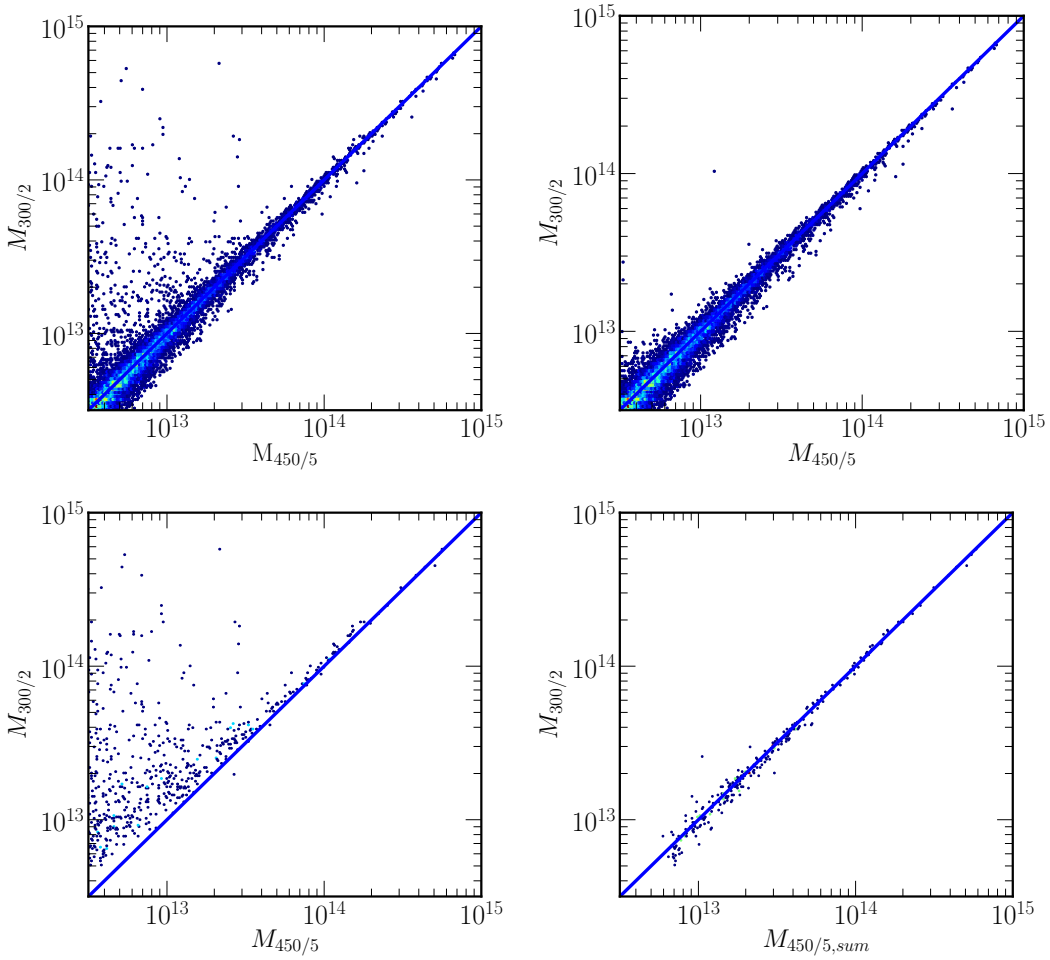

Figure 7. Comparison of halo masses matching the 450/5 (x-axis) to the 300/2 (y-axis) simulation at $z = 0.15$. Panels correspond to halos with different matching criteria: all the matched halos (top left), matched halos having one-to-one correspondence (top right), matched halos not having one-to-one correspondence called "multiply-booked" halos (bottom left), and the "multiply-booked" halos whose corresponding halo masses are added (bottom right). Those panels imply that large mass difference between the 450/5 and the 300/2 shown in the top left panel is mainly due to those "multiply-booked" halos and that the corresponding "multiply-booked" halos in the 450/5 are merged into one halo in the 300/2 due to larger time steps.

global steps, the results are significantly improved and the center position is matched in these cases to better than 200 kpc. As is clear from Figure 9, the difference between 3 and 2 sub-cycles is negligible on halo properties. The same results shown in Figure 9 but for other redshifts are in Table 3 and 4. They support the same argument discussed for Figure 9. Table 4 shows fractions of halos whose velocity directions are matched to the ones for the 450/5 within 10 degree. More than 90% of the matched halos have angles between the velocities within 10 degree at all the redshifts, $z = 0.15$, $z = 0.5$, and $z = 0.8$.

As a conclusion through several convergence tests shown in this section, we determine 300/2 as our optimal choice.

3 TUNING 300/2

In the previous section, we choose 300/2 as our final target for the time-stepping scheme. Now, we need to take a close look at observable quantities

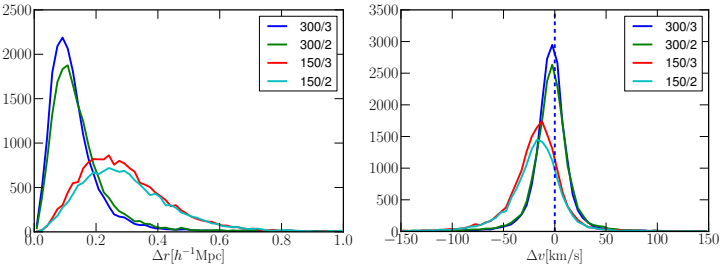

[t]

Figure 9. Comparison of matched halos in the different simulations corresponding to 300/3 (blue), 300/2 (green), 150/3 (red), and 150/2 (cyan) with respect to the 450/5. From left to right, we compared halo position and velocity respectively. The agreement between 300 global steps and the 450/5 is considerably good, with little difference from the number of sub-cycles.

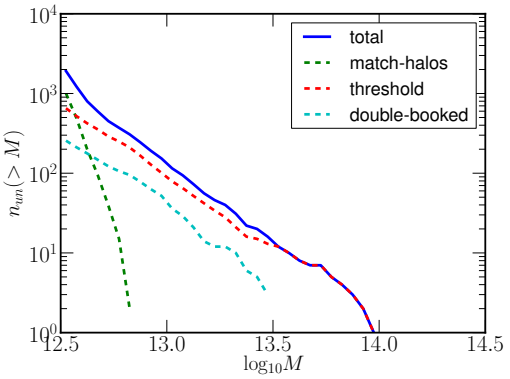

Figure 8. Itemization of unmatched halos shown as cumulative number densities of the unmatched halos from each procedure in the matching algorithm. The solid line is the total and the dashed lines correspond to matching based on particle content (green), elimination due to the matching threshold (red), and elimination of "multiply-booked" halos which are sub halos (cyan). Most large halos being unmatched is due to the threshold.

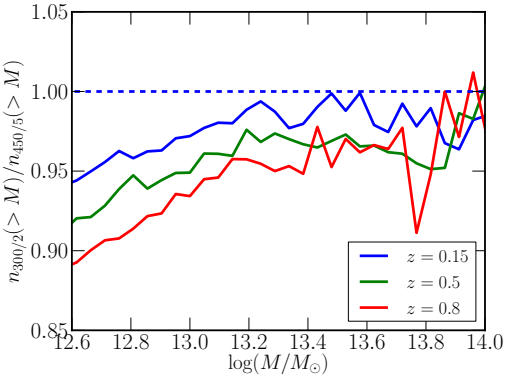

Figure 10. Comparison of cumulative mass functions between 450/5 and 300/2 at $z = 0.15$, $z = 0.5$, and $z = 0.8$. For the larger redshifts, the deviation gets larger particularly on small halo masses.

calculated from the samples of 300/2 at various redshifts. Here, we first compare cumulative mass functions between 450/5 and 300/2 at redshifts $z = 0.15$, $z = 0.5$, and $z = 0.8$ corresponding to different colors shown in Figure 10. As shown, an offset from one increases with higher redshifts, particularly on small halo masses. To make the mass functions for 300/2 closer to the ones for 450/5, we decided to reassign halo masses for halos in the simulations of 300/2.

3.1 method

In order to compare halo mass differences between 300/2 and 450/5, we first match halos in the 300/2 simulation to halos in the 450/5 by using our matching algorithm. Next, we take mean of the halo mass differences for those matched halos as a function of halo mass of 300/2 and fit the mean to a functional shown below,

$$M_{re} = M_{300/2}(1.0 + \alpha(M_{300/2}/10^{12.0}[\mathrm{M}_\odot])^\beta, \quad (2)$$

where M_{re} is a reassigned halo mass for the samples of 300/2, $M_{300/2}$ is an original halo mass of 300/2, α and β are free parameters which are functions of the redshift. By fitting to the samples of 300/2 to the 450/5 by using the above functional, we find best fit parameters shown below:

$$\alpha(z) = 0.123z + 0.052, \quad (3)$$

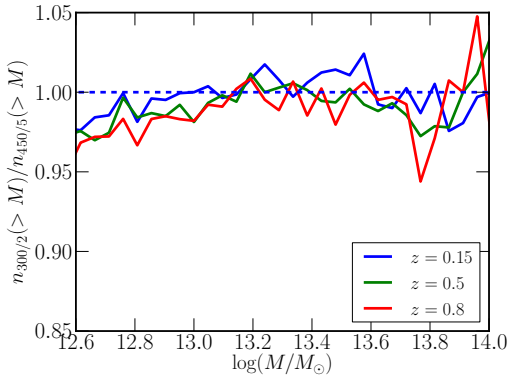

Figure 11. Comparison of cumulative mass functions after reassigning halo masses for the simulation of 300/2. The agreement of 300/2 with 450/5 is significantly improved especially on halo masses greater than $10^{13.0}\mathrm{M}_\odot$.

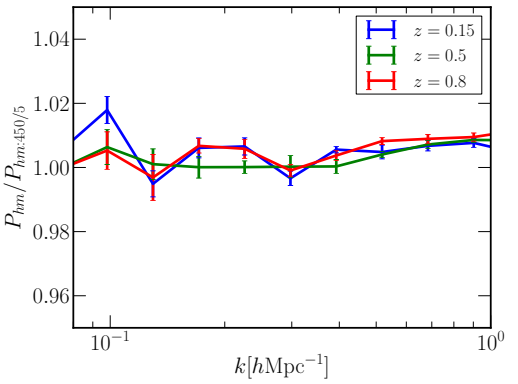

Figure 12. Ratio of halo-matter cross power spectra after reassigning halo masses for the sample from the 300/2 simulations. We select halos based on the soft mass-cut method with $M_{cut} = 13.0$ and $\sigma = 0.5$. The overall agreements are well within 2%.

and

$$\beta(z) = -0.154z - 0.447. \quad (4)$$

Applying the functional to the samples from 300/2, we obtain mass functions shown in Figure 11. The match of reassigned halo mass functions for 300/2 to the 450/5 mass functions is significantly improved that now the difference is well within 5% on any halo masses at any redshifts.

3.2 Power Spectra

We calculate halo-matter cross power spectra after reassigning halo masses for 300/2, as shown in Figure 12. We use halo mass thresholds of $10^{12.5}\mathrm{M}_\odot$ for the left panel and $10^{13.0}\mathrm{M}_\odot$ for the right panel. As expected from the mass functions, the match between 300/2 and 450/5 with the threshold of $10^{13.0}\mathrm{M}_\odot$ is better than the one with $10^{12.5}\mathrm{M}_\odot$. The agreement between 300/2 and 450/5 is, however, well within 2% for both cases, which is a significant improvement compared to the results shown in the previous section.

[h] Table: $\log_{10}(M/M_{450/5})$

z=0.15	median	$\Delta_{65\%}$	$\Delta_{95\%}$
300/3	-0.0026	0.0877	0.2864
300/2	-0.0078	0.0972	0.3458
150/3	-0.0266	0.1107	0.3101
150/2	-0.0454	0.1207	0.3315

z=0.5	median	$\Delta_{65\%}$	$\Delta_{95\%}$
300/3	-0.0062	0.0905	0.2869
300/2	-0.0139	0.1029	0.3345
150/3	-0.0372	0.1148	0.3083
150/2	-0.0595	0.1252	0.3093

z=0.8	median	$\Delta_{65\%}$	$\Delta_{95\%}$
300/3	-0.0067	0.0932	0.2891
300/2	-0.0189	0.1048	0.3347
150/3	-0.0519	0.1172	0.2926
150/2	-0.0782	0.1274	0.28878

Table 1. Comparison of halo mass ratios $\log_{10}M/M_{450/5}$ in log-based, comparing various time steps to the 450/5 simulation at $z = 0.15$, $z = 0.5$, and $z = 0.8$. For each redshift, we report median, $\Delta_{95\%}$, and $\Delta_{65\%}$ (how should I explain about $\Delta_{95\%}$?). As shown in Figure 9, the results indicate that mass ratio distributions for the 300 global steps have less scatter than for the 150 global steps.

[H]

z=0.15	median	$\Delta_{65\%}$	$\Delta_{95\%}$
$M_{halo} \in [10^{12.5}, 10^{13.0}]$	-0.0111	0.1124	0.3896
$M_{halo} \in [10^{13.0}, 10^{13.5}]$	-0.0085	0.0748	0.2599
$M_{halo} \in [10^{13.5}, 10^{14.0}]$	-0.0056	0.0471	0.1596
$M_{halo} > 10^{14.0}$	-0.0047	0.0341	0.1323

z=0.5	median	$\Delta_{65\%}$	$\Delta_{95\%}$
$M_{halo} \in [10^{12.5}, 10^{13.0}]$	-0.0197	0.1156	0.3544
$M_{halo} \in [10^{13.0}, 10^{13.5}]$	-0.0123	0.0790	0.2546
$M_{halo} \in [10^{13.5}, 10^{14.0}]$	-0.0067	0.0497	0.1813
$M_{halo} > 10^{14.0}$	-0.0052	0.0309	0.0731

z=0.8	median	$\Delta_{65\%}$	$\Delta_{95\%}$
$M_{halo} \in [10^{12.5}, 10^{13.0}]$	-0.0260	0.1161	0.3478
$M_{halo} \in [10^{13.0}, 10^{13.5}]$	-0.0167	0.0835	0.2546
$M_{halo} \in [10^{13.5}, 10^{14.0}]$	-0.0084	0.0490	0.1809
$M_{halo} > 10^{14.0}$	-0.0077	0.0297	0.1361

Table 2. Comparison of halo mass ratios $\log_{10}M_{300/2}/M_{450/5}$ in log-based, comparing the 300/2 to the 450/5 simulation as a function of halo mass slices at $z = 0.15$, $z = 0.5$, and $z = 0.8$. For each redshift, we report median, $\Delta_{95\%}$, and $\Delta_{65\%}$. As shown, medians and Δs decreases as increasing halo mass and decreasing redshift.

[H]

z=0.15	median	$\Delta_{65\%}$	$\Delta_{95\%}$
300/3	0.1116	0.1228	0.4439
300/2	0.1245	0.1406	0.5558
150/3	0.2706	0.2571	0.6234
150/2	0.2800	0.2680	0.6568

z=0.5	median	$\Delta_{65\%}$	$\Delta_{95\%}$
300/3	0.1221	0.1298	0.4700
300/2	0.1348	0.1460	0.5400
150/3	0.2382	0.2248	0.5555
150/2	0.2475	0.2335	0.5835

z=0.8	median	$\Delta_{65\%}$	$\Delta_{95\%}$
300/3	0.1217	0.1329	0.4553
300/2	0.1354	0.1498	0.4969
150/3	0.2447	0.2284	0.5408
150/2	0.2536	0.2334	0.5418

Table 3. Comparison of halo positions for various time steps to the 450/5 simulation at $z = 0.15$, $z = 0.5$, and $z = 0.8$. For each redshift, we report median, $\Delta_{95\%}$, and $\Delta_{65\%}$. As shown, the halo positions for the 150 global steps are more scattered and 3 and 2 sub-cycles affect negligibly on halo positions. Also, there is little change due to redshift.

z=0.15	median	$\Delta_{65\%}$	$\Delta_{95\%}$
300/3	-3.36	24.3872	82.20
300/2	-3.26	27.5063	99.40
150/3	-16.61	38.4702	116.93
150/2	-17.05	39.9572	121.45

z=0.5	median	$\Delta_{65\%}$	$\Delta_{95\%}$
300/3	-3.78	36.87	118.48
300/2	-3.94	40.77	137.62
150/3	-23.25	53.41	151.75
150/2	-24.26	56.75	160.15

z=0.8	median	$\Delta_{65\%}$	$\Delta_{95\%}$
300/3	-6.32	47.41	149.72
300/2	-6.47	53.48	169.1556
150/3	-25.23	67.62	186.29
150/2	-24.76	71.97	189.26

Table 4. Comparison of halo velocity for various time steps to the 450/5 simulation at $z = 0.15$, $z = 0.5$, and $z = 0.8$. For each redshift, we report median, $\Delta_{95\%}$, and $\Delta_{65\%}$. As shown in Figure 9, the results indicate that mass ratio distributions for the 300 global steps have less scatter than for the 150 global steps.

z=0.15	fraction within 10 degree
300/3	0.951
300/2	0.938
150/3	0.928
150/2	0.923

Table 5. Fractions of halos whose velocity direction matches with the 450/5 within 10 degree at $z = 0.15$. More than 90% f halos for any time steps agree with the 450/5 simulation.